AIAA JOURNAL
Vol. 46, No. 5, May 2008

Continuous Adjoint Method for Unstructured Grids

Antony Jameson* and Sriram Shankaran†
Stanford University, Stanford, California 94305-4035
and
Luigi Martinelli‡
Princeton University, Princeton, New Jersey 08544

DOI: 10.2514/1.25362

Adjoint-based shape optimization methods have proven to be computationally efficient for aerodynamic problems. The majority of the studies on adjoint methods have used structured grids to discretize the computational domain. Because of the potential advantages of unstructured grids for complex configurations, in this study we have developed and validated a continuous adjoint formulation for unstructured grids. The hurdles posed in the computation of the gradient for unstructured grids are resolved by using a reduced gradient formulation. The methods to impose thickness constraints on unstructured grids are also discussed. The results for two- and three-dimensional simulations of airfoils and wings in inviscid transonic flow are used to validate the design procedure. Finally, the design procedure is applied to redesign the shape of a transonic business jet configuration; we were able to reduce the inviscid drag of the aircraft from 235 to 216 counts resulting in a shock-free wing. Although the Euler equations are the focus of the study in this paper of the adjoint-based approach, the solution of the adjoint system and gradient formulation can be conceptually extended to viscous flows. The approach presented in this study has been successfully used by the first and third authors for viscous flows using structured grids. However, particular aspects of the design process, such as the robustness of the mesh deformation process for unstructured grids, need more attention for viscous flows and are therefore the subject of ongoing research.

Nomenclature

A_i = Jacobian of the Euler fluxes
$\mathcal{B}$ = boundary of the computational domain
$\mathcal{B}_F$ = boundary of the computational domain containing the far field
$\mathcal{B}_W$ = boundary of the computational domain containing the wing surface
c = speed of sound
$\mathcal{D}$ = computational domain
D_o = numerical dissipation at node o
E = total energy
E_o = difference of the state vector along edge ko
F = function to represent the boundary shape
f_i = convective flux term of the Euler equation
$\mathcal{G}$ = gradient
H = enthalpy
I = cost function
K_{ij} = elements of the transformation matrix
n_i = unit outward normal at the boundary
p = pressure
p_d = desired pressure distribution
p_t = target pressure distribution
q = dynamic pressure
R = Euler or Navier–Stokes operator
R_k = discrete residual at node k
S = boundary of the control volume
S_{ij} = cofactors of the transformation matrix
S_x = component of the normal to the boundary of the control volume in the x direction
S_y = component of the normal to the boundary of the control volume in the y direction
S_z = component of the normal to the boundary of the control volume in the z direction
u_i = velocity components
V = control volume
w = state vector for the equations
x_i = computational coordinates
Δx_i = displacement of node i
γ = specific heat ratio
$\epsilon^{(1)}_{ko}$ = coefficient of first-order dissipation for edge ko
$\epsilon^{(2)}_{ko}$ = coefficient of third-order dissipation for edge ko
ξ_i = transformed coordinates
ρ = density
ϕ = arbitrary differentiable test function
ψ = Lagrange multiplier

I. Introduction

WITH the availability of high-performance computing platforms and robust numerical methods to simulate fluid flows, it is possible to shift attention to the automated design procedures that combine computational fluid dynamics (CFD) with optimization techniques to determine optimum aerodynamic designs. The feasibility of this is by now well established[1–6], and it is actually possible to calculate optimum three-dimensional transonic wing shapes in a few hours, accounting for viscous effects with the flow modeled by the Reynolds-averaged Navier–Stokes equations. By enforcing the constraints on the thickness and span-load distribution, one can make sure that there is no penalty in structure weight or fuel volume. Larger scale shape changes, such as planform variations, can also be accommodated [7]. It then becomes necessary to include a structural weight model to enable a proper compromise between minimum drag and low structure weight to be determined.

Aerodynamic shape optimization has been successfully performed for a variety of complex configurations using multiblock structured meshes [8,9]. Meshes of this type can be relatively easily

Presented as Paper 3955 at the 16th AIAA CFD Conference, Orlando, FL, 23–26 June 2006; received 22 May 2006; accepted for publication 23 December 2006.

*Thomas V. Jones Professor, Department of Aeronautics and Astronautics, School of Engineering, Durand Building, 496 Lomita Mall.
†Postdoctoral Research Associate, School of Engineering, Durand Building, 496 Lomita Mall.
‡Professor, Department of Mechanical and Aerospace Engineering, D 216 E-Quad.

deformed to accommodate the shape variations required in the redesign. However, it is both extremely time consuming and expensive in human costs to generate such meshes. Consequently, we believe it is essential to develop shape optimization methods that use unstructured meshes for the flow simulation.

Typically, in gradient-based optimization techniques, a control function to be optimized (the wing shape, for example) is parameterized with a set of design variables, and a suitable cost function to be minimized is defined. For aerodynamic problems, the cost function is typically lift, drag, or a specified target pressure distribution. Then, a constraint, the governing equations, can be introduced to express the dependence between the cost function and the control function. The sensitivity derivatives of the cost function with respect to the design variables are calculated to get a direction of improvement. Finally, a step is taken in this direction and the procedure is repeated until convergence is achieved. Finding a fast and accurate way of calculating the necessary gradient information is essential to developing an effective design method, because this can be the most time-consuming portion of the design process. This is particularly true in problems that involve a very large number of design variables, as is the case in a typical three-dimensional shape optimization.

The control theory approach [1,10,11] has dramatic computational cost advantages over the finite difference method of calculating gradients. With this approach, the necessary gradients are obtained through the solution of an adjoint system of equations of the governing equations of interest. The adjoint method is extremely efficient, because the computational expense incurred in the calculation of the complete gradient is effectively independent of the number of design variables.

In this study, a continuous adjoint formulation has been used to derive the adjoint system of equations. Accordingly, the adjoint equations are derived directly from the governing equations and then discretized. This approach has the advantage over the discrete adjoint formulation in that the resulting adjoint equations are independent of the form of discretized flow equations. The adjoint system of equations has a similar form to the governing equations of the flow and, hence, the numerical methods developed for the flow equations [12–14] can be reused for the adjoint equations.

The gradient is derived solely from the adjoint solution and the surface displacement, independent of the mesh modification. This is crucial for unstructured meshes. If the gradient depends on the form of the mesh modification, then the field integral in the gradient calculation has to be recomputed for mesh modifications corresponding to each design variable. This would be prohibitively expensive if the geometry is treated as a free surface defined by the mesh points. Consequently, to reduce the computational cost with this approach [15–17], the number of design variables would have to be reduced by parameterizing the geometry. However, this reduced set of design variables could not recover all possible shape variations.

A steepest descent method is finally used to improve the initial design. To guarantee that the shape variations remain sufficiently smooth, the gradients are redefined so that they correspond to an inner product in a Sobolev space. This is accomplished by an implicit smoothing procedure that also acts as an effective preconditioner, with the result that the number of design steps needed to reach an optimum is quite small, of the order of 20–50.

II. General Formulation of Adjoint Approach to Optimal Design

For flow about an airfoil, or wing, the aerodynamic properties that define the cost function are functions of the flowfield variables and the physical location of the boundary. Then,

$$I = I(w, \mathcal{F})$$

and a change in $\mathcal{F}$ results in a change

$$\delta I = \frac{\partial I^T}{\partial w}\delta w + \frac{\partial I^T}{\partial \mathcal{F}}\delta \mathcal{F} \tag{1}$$

in the cost function. Using control theory, the governing equations of the flowfield are introduced as a constraint in such a way that the final expression for the gradient does not require reevaluation of the flowfield. To achieve this, δw must be eliminated from Eq. (1). Suppose that the governing equation R, which expresses the dependence of w and $\mathcal{F}$ within the flowfield domain D, can be written as

$$R(w, \mathcal{F}) = 0 \tag{2}$$

Then δw is determined from the equation

$$\delta R = \left[\frac{\partial R}{\partial w}\right]\delta w + \left[\frac{\partial R}{\partial \mathcal{F}}\right]\delta \mathcal{F} = 0 \tag{3}$$

Next, introducing a Lagrange multiplier ψ, we have

$$\delta I = \frac{\partial I^T}{\partial w}\delta w + \frac{\partial I^T}{\partial \mathcal{F}}\delta \mathcal{F} - \psi^T\left(\left[\frac{\partial R}{\partial w}\right]\delta w + \left[\frac{\partial R}{\partial \mathcal{F}}\right]\delta \mathcal{F}\right)$$

$$\delta I = \left(\frac{\partial I^T}{\partial w} - \psi^T\left[\frac{\partial R}{\partial w}\right]\partial w\right)\delta w + \left(\frac{\partial I^T}{\partial \mathcal{F}} - \psi^T\left[\frac{\partial R}{\partial \mathcal{F}}\right]\delta \mathcal{F}\right)$$

Choosing ψ to satisfy the adjoint equation

$$\left[\frac{\partial R}{\partial w}\right]^T \psi = \frac{\partial I}{\partial w} \tag{4}$$

the first term is eliminated and we find that

$$\delta I = \mathcal{G}\delta \mathcal{F} \tag{5}$$

where

$$\mathcal{G} = \frac{\partial I^T}{\partial \mathcal{F}} - \psi^T\left[\frac{\partial R}{\partial \mathcal{F}}\right] \tag{6}$$

This process allows for the elimination of the terms that depend on the flow solution, with the result that the gradient with respect to an arbitrary number of design variables can be determined without the need for additional flowfield evaluations.

After taking a step in the negative gradient direction, the gradient is recalculated and the process repeated to follow the path of steepest descent until a minimum is reached. To avoid violating constraints, such as the minimum acceptable wing thickness, the gradient can be projected into an allowable subspace within which the constraints are satisfied. In this way, one can devise procedures that must necessarily converge at least to a local minimum and that can be accelerated by the use of more sophisticated descent methods, such as conjugate gradient or quasi-Newton algorithms. There is a possibility of more than one local minimum but, in any case, this method will lead to an improvement over the original design.

III. Design Using Euler Equations

The application of control theory to aerodynamic design problems is illustrated in this section for the case of a three-dimensional wing design using the compressible Euler equations as the mathematical model. It proves convenient to denote the Cartesian coordinates and velocity components by x_1, x_2, x_3 and u_1, u_2, u_3 and to use the convention that summation over $i = 1$ to 3 is implied by a repeated index i. Then, the three-dimensional Euler equations may be written as

$$\frac{\partial w}{\partial t} + \frac{\partial f_i}{\partial x_i} = 0 \quad \text{in } D \tag{7}$$

where

$$w = \begin{Bmatrix} \rho \\ \rho u_1 \\ \rho u_2 \\ \rho u_3 \\ \rho E \end{Bmatrix}, \qquad f_i = \begin{Bmatrix} \rho u_i \\ \rho u_i u_1 + p\delta_{i1} \\ \rho u_i u_2 + p\delta_{i2} \\ \rho u_i u_3 + p\delta_{i3} \\ \rho u_i H \end{Bmatrix} \tag{8}$$

and δ_{ij} is the Kronecker delta function. Also,

$$p = (\gamma - 1)\rho\left\{E - \tfrac{1}{2}(u_i^2)\right\} \tag{9}$$

and

$$\rho H = \rho E + p \tag{10}$$

where γ is the ratio of the specific heats.

Consider a transformation to coordinates ξ_1, ξ_2, ξ_3 where

$$K_{ij} = \left[\frac{\partial x_i}{\partial \xi_j}\right], \qquad J = \det(K), \qquad K_{ij}^{-1} = \left[\frac{\partial \xi_i}{\partial x_j}\right]$$

and

$$S = JK^{-1}$$

The elements of S are the cofactors of K and, in a finite volume discretization, they are just the face areas of the computational cells projected in the x_1, x_2, and x_3 directions. Using the permutation tensor ϵ_{ijk} we can express the elements of S as

$$S_{ij} = \frac{1}{2}\epsilon_{jpq}\epsilon_{irs}\frac{\partial x_p}{\partial \xi_r}\frac{\partial x_q}{\partial \xi_s} \tag{11}$$

Then

$$\frac{\partial}{\partial \xi_i} S_{ij} = \frac{1}{2}\epsilon_{jpq}\epsilon_{irs}\left(\frac{\partial^2 x_p}{\partial \xi_r \partial \xi_i}\frac{\partial x_q}{\partial \xi_s} + \frac{\partial x_p}{\partial \xi_r}\frac{\partial^2 x_q}{\partial \xi_s \partial \xi_i}\right) = 0 \tag{12}$$

Now, multiplying Eq. (7) by J and applying the chain rule,

$$J\frac{\partial w}{\partial t} + R(w) = 0 \tag{13}$$

where

$$R(w) = S_{ij}\frac{\partial f_j}{\partial \xi_i} = \frac{\partial}{\partial \xi_i}(S_{ij} f_j) \tag{14}$$

using Eq. (12). We can write the transformed fluxes in terms of the scaled contravariant velocity components

$$U_i = S_{ij} u_j$$

as

$$F_i = S_{ij} f_j = \begin{bmatrix} \rho U_i \\ \rho U_i u_1 + S_{i1} p \\ \rho U_i u_2 + S_{i2} p \\ \rho U_i u_3 + S_{i3} p \\ \rho U_i H \end{bmatrix}$$

Assume now that the new computational coordinate system conforms to the wing in such a way that the wing surface B_W is represented by $\xi_2 = 0$. Then the flow is determined as the steady-state solution of Eq. (13) subject to the flow tangency condition

$$U_2 = 0 \quad \text{on} \quad B_W \tag{15}$$

At the far-field boundary B_F, conditions are specified for incoming waves, as in the two-dimensional case, whereas outgoing waves are determined by the solution.

The weak form of the Euler equations for steady flow can be written as

$$\int_{\mathcal{D}} \frac{\partial \phi^T}{\partial \xi_i} F_i \, \mathrm{d}\mathcal{D} = \int_{\mathcal{B}} n_i \phi^T F_i \, \mathrm{d}\mathcal{B} \tag{16}$$

where the test vector ϕ is an arbitrary differentiable function and n_i is the outward normal at the boundary. If a differentiable solution w is obtained to this equation, it can be integrated by parts to give

$$\int_{\mathcal{D}} \phi^T \frac{\partial F_i}{\partial \xi_i} \, \mathrm{d}\mathcal{D} = 0$$

and because this is true for any ϕ, the differential form can be recovered. If the solution is discontinuous, Eq. (16) may be integrated by parts separately on either side of the discontinuity to recover the shock jump conditions.

Suppose now that it is desired to control the surface pressure by varying the wing shape. For this purpose, it is convenient to retain a fixed computational domain. Then variations in the shape result in corresponding variations in the mapping derivatives defined by K. As an example, consider the case of an inverse problem, in which we introduce the cost function

$$I = \frac{1}{2}\iint_{B_W} (p - p_d)^2 \, \mathrm{d}\xi_1 \, \mathrm{d}\xi_3$$

where p_d is the desired pressure. The design problem is now treated as a control problem in which the control function is the wing shape, which is to be chosen to minimize I subject to the constraints defined by the flow equations (13). A variation in the shape will cause a variation δp in the pressure and, consequently, a variation in the cost function

$$\delta I = \iint_{B_W} (p - p_d)\delta p \, \mathrm{d}\xi_1 \, \mathrm{d}\xi_3 + \frac{1}{2}\int_{\mathcal{B}} (p - p_t)^2 \, \mathrm{d}\delta S \tag{17}$$

where typically the second term is negligible and can be dropped.

Because p depends on w through the equation of state (9) and (10), the variation δp can be determined from the variation δw. Define the Jacobian matrices

$$A_i = \frac{\partial f_i}{\partial w}, \qquad C_i = S_{ij} A_j \tag{18}$$

The weak form of the equation for δw in the steady state becomes

$$\int_{\mathcal{D}} \frac{\partial \phi^T}{\partial \xi_i} \delta F_i \, \mathrm{d}\mathcal{D} = \int_{\mathcal{B}} (n_i \phi^T \delta F_i) \, \mathrm{d}\mathcal{B}$$

where

$$\delta F_i = C_i \delta w + \delta S_{ij} f_j$$

which should hold for any differential test function ϕ. This equation may be added to the variation in the cost function, which may now be written as

$$\delta I = \iint_{B_W} (p - p_d)\delta p \, \mathrm{d}\xi_1 \, \mathrm{d}\xi_3 - \int_{\mathcal{D}} \left(\frac{\partial \phi^T}{\partial \xi_i}\delta F_i\right) \mathrm{d}\mathcal{D} + \int_{\mathcal{B}} (n_i \phi^T \delta F_i) \, \mathrm{d}\mathcal{B} \tag{19}$$

On the wing surface B_W, $n_1 = n_3 = 0$. Thus, it follows from Eq. (15) that

$$\delta F_2 = \begin{bmatrix} 0 \\ S_{21}\delta p \\ S_{22}\delta p \\ S_{23}\delta p \\ 0 \end{bmatrix} + \begin{bmatrix} 0 \\ \delta S_{21} p \\ \delta S_{22} p \\ \delta S_{23} p \\ 0 \end{bmatrix} \tag{20}$$

Because the weak equation for δw should hold for an arbitrary choice of the test vector ϕ, we are free to choose ϕ to simplify the resulting expressions. Therefore, we set $\phi = \psi$, where the costate vector ψ is the solution of the adjoint equation

$$\frac{\partial \psi}{\partial t} - C_i^T \frac{\partial \psi}{\partial \xi_i} = 0 \quad \text{in } D \tag{21}$$

At the outer boundary, incoming characteristics for ψ correspond to outgoing characteristics for δw. Consequently, one can choose boundary conditions for ψ such that

$$n_i \psi^T C_i \delta w = 0$$

Then, if the coordinate transformation is such that δS is negligible in the far field, the only remaining boundary term is

$$-\iint_{B_W} \psi^T \delta F_2 \, \mathrm{d}\xi_1 \, \mathrm{d}\xi_3$$

Thus, by letting ψ satisfy the boundary condition,

$$S_{21}\psi_2 + S_{22}\psi_3 + S_{23}\psi_4 = (p - p_d) \quad \text{on } B_W \tag{22}$$

we find finally that

$$\delta I = -\int_{\mathcal{D}} \frac{\partial \psi^T}{\partial \xi_i} \delta S_{ij} f_j \, \mathrm{d}\mathcal{D} - \iint_{B_W} (\delta S_{21}\psi_2 + \delta S_{22}\psi_3 + \delta S_{23}\psi_4) p \, \mathrm{d}\xi_1 \, \mathrm{d}\xi_3 \tag{23}$$

Here the expression for the cost variation depends on the mesh variations throughout the domain that appear in the field integral. However, the true gradient for a shape variation should not depend on the way in which the mesh is deformed, but only on the true flow solution. In Sec. IV, we show how the field integral can be eliminated to produce a reduced gradient formula that depends only on the boundary movement.

IV. Reduced Gradient Formulations

Continuous adjoint formulations have generally used a form of the gradient that depends on the manner in which the mesh is modified for perturbations in each design variable. To represent all possible shapes, the control surface should be regarded as a free surface. If the surface mesh points are used to define the surface, this leaves the designer with thousands of design variables. On an unstructured mesh, evaluating the gradient by perturbing each design variable in turn would be prohibitively expensive because of the need to determine the corresponding perturbations of the entire mesh. This would inhibit the use of this design tool in any meaningful design process.

To avoid this difficulty, an alternate formulation to the gradient calculation is followed in this study. This idea was developed by Jameson and Kim [18] and was validated for two- and three-dimensional problems with structured grids. However, as it is possible to devise mesh modification routines that are computationally cheap on structured grids, the major benefit of this alternate gradient formulation is for general three-dimensional unstructured grids. To complete the formulation of the control theory approach to shape optimization, the gradient formulations are outlined next. The formulation for the reduced gradients in the continuous limit is presented in the context of the transformation between the physical domain and the computational domain and is easily extended to unstructured grid methods in which these transformations are not explicitly used.

The evaluation of the field integral in Eq. (23) requires the evaluation of the metric variations δS_{ij} throughout the domain. However, the true gradient should not depend on the way the mesh is modified.

Consider the case of a mesh variation with a fixed boundary. Then,

$$\delta I = 0$$

but there is a variation in the transformed flux,

$$\delta F_i = C_i \delta w + \delta S_{ij} f_j$$

Here the true solution is unchanged. Thus, the variation δw is due to the mesh movement δx in a fixed boundary configuration. Therefore,

$$\delta w = \nabla w \cdot \delta x = \frac{\partial w}{\partial x_j} \delta x_j (= \delta w^*)$$

and because

$$\frac{\partial}{\partial \xi_i} \delta F_i = 0$$

it follows that

$$\frac{\partial}{\partial \xi_i} (\delta S_{ij} f_j) = -\frac{\partial}{\partial \xi_i} (C_i \delta w^*) \tag{24}$$

It is verified in Jameson and Kim [18] that this relation holds in the general case with boundary movement. Now

$$\int_{\mathcal{D}} \psi^T \delta R \, \mathrm{d}\mathcal{D} = \int_{\mathcal{D}} \psi^T \frac{\partial}{\partial \xi_i} C_i (\delta w - \delta w^*) \, \mathrm{d}\mathcal{D} = \int_{\mathcal{B}} \psi^T C_i (\delta w - \delta w^*) \, \mathrm{d}\mathcal{B} - \int_{\mathcal{D}} \frac{\partial \psi^T}{\partial \xi_i} C_i (\delta w - \delta w^*) \, \mathrm{d}\mathcal{D} \tag{25}$$

Here on the wall boundary

$$C_2 \delta w = \delta F_2 - \delta S_{2j} f_j \tag{26}$$

Thus, by choosing ψ to satisfy the adjoint equation and the adjoint boundary condition, we have finally the cost variation that is reduced to a boundary integral

$$\delta I = \int_{\mathcal{B}_W} \psi^T (\delta S_{2j} f_j + C_2 \delta w^*) \, \mathrm{d}\xi_1 \, \mathrm{d}\xi_3 - \iint_{B_W} (\delta S_{21}\psi_2 + \delta S_{22}\psi_3 + \delta S_{23}\psi_4) p \, \mathrm{d}\xi_1 \, \mathrm{d}\xi_3 \tag{27}$$

In this reduced formulation, the cost variation depends only on the boundary shape variations, with the result that the gradient can be evaluated without any knowledge of the mesh deformation.

Another key issue for the successful implementation of the continuous adjoint method is the choice of an appropriate inner product for the definition of the gradient. It turns out that there is an enormous benefit from the use of a modified Sobolev gradient, which enables the generation of a sequence of smooth shapes. This can be illustrated by considering a simple problem in calculus of variations.

Choose $y(x)$ to minimize

$$I = \int_a^b F(y, y') \, \mathrm{d}x$$

with fixed end points $y(a)$ and $y(b)$. Under a variation $\delta y(x)$,

$$\delta I = \int_a^b \left(\frac{\partial F}{\partial y} \delta y + \frac{\partial F}{\partial y'} \delta y' \right) \mathrm{d}x = \int_a^b \left(\frac{\partial F}{\partial y} - \frac{\mathrm{d}}{\mathrm{d}x} \frac{\partial F}{\partial y'} \right) \delta y \, \mathrm{d}x$$

Thus, defining the gradient as

$$g = \frac{\partial F}{\partial y} - \frac{\mathrm{d}}{\mathrm{d}x} \frac{\partial F}{\partial y'}$$

and the inner product as

$$(u, v) = \int_a^b uv \, \mathrm{d}x$$

we find that

$$\delta I = (g, \delta y)$$

Then, if we set

$$\delta y = -\lambda g, \qquad \lambda > 0$$

we obtain an improvement,

$$\delta I = -\lambda(g, g) \leq 0$$

unless $g = 0$, the necessary condition for a minimum. Note that g is a function of y, y', and y'':

$$g = g(y, y', y'')$$

In the case of the Brachistrone problem, for example,

$$g = -\frac{1 + y'^2 + 2yy''}{2(y(1 + y'^2))^{3/2}}$$

Now each step

$$y^{n+1} = y^n - \lambda^n g^n$$

reduces the smoothness of y by 2 classes. Thus, the computed trajectory becomes less and less smooth, leading to instability.

To prevent this, we can introduce a modified Sobolev inner product [19]:

$$\langle u, v \rangle = \int (uv + \epsilon u'v') \, \mathrm{d}x$$

where ϵ is a parameter that controls the weight of the derivatives. If we define a gradient $\bar{g}$ such that

$$\delta I = \langle \bar{g}, \delta y \rangle$$

Then we have

$$\delta I = \int (\bar{g}\delta y + \epsilon \bar{g}' \delta y') \, \mathrm{d}x = \int \left(\bar{g} - \frac{\partial}{\partial x} \epsilon \frac{\partial \bar{g}}{\partial x} \right) \delta y \, \mathrm{d}x = (g, \delta y)$$

where

$$\bar{g} - \frac{\partial}{\partial x} \epsilon \frac{\partial \bar{g}}{\partial x} = g$$

and $\bar{g} = 0$ at the end points. Thus, $\bar{g}$ is obtained from g by a smoothing equation.

Now the step

$$y^{n+1} = y^n - \lambda^n \bar{g}^n$$

gives an improvement,

$$\delta I = -\lambda^n \langle \bar{g}^n, \bar{g}^n \rangle$$

but y^{n+1} has the same smoothness as y^n, resulting in a stable process.

In applying control theory for aerodynamic shape optimization, the use of a Sobolev gradient is equally important for the preservation of the smoothness class of the redesigned surface; we have employed it to obtain all the results in this study.

V. Imposing Thickness Constraints on Unstructured Meshes

To perform meaningful drag reduction computations, it is necessary to ensure that constraints such as the thickness of the wing are satisfied during the design process. On an arbitrary unstructured mesh, there appears to be no straightforward way to impose thickness constraints. In our approach, we introduce cutting planes at various spanwise locations along the wing and transform the airfoil sections to shallow bumps by a square root mapping. Then we interpolate the gradients from the nodes on the surface to the airfoil sections on the cutting planes and impose the thickness constraints on the mapped sections. The displacements of the points on the surface of the CFD mesh are obtained by interpolation from the mapped airfoil sections and transformed back to the physical domain by a reverse mapping.

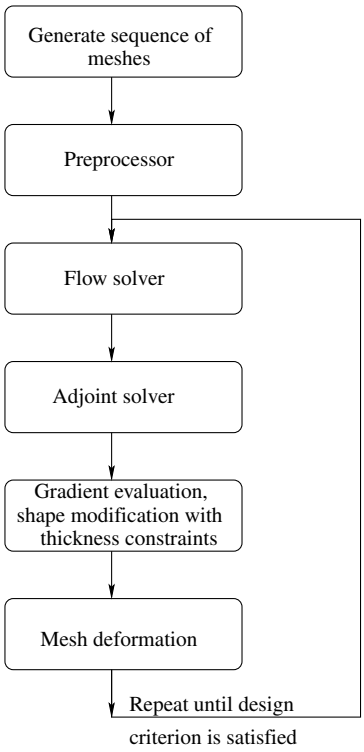

Fig. 1 Flow chart of the overall design process.

These surface displacements are finally used as inputs to a mesh deformation algorithm.

VI. Mesh Deformation

The modifications to the shape of the boundary are transferred to the volume mesh using the spring method. This approach has been found to be adequate for the computations performed in this study.

The spring method can be mathematically conceptualized as solving the following equation:

$$\frac{\partial \Delta x_i}{\partial t} + \sum_{j=1}^{N} K_{ij}(\Delta x_i - \Delta x_j) = 0$$

where K_{ij} is the stiffness of the edge connecting node i to node j and its value is inversely proportional to the length of this edge; Δx_i is the displacement of node i; and Δx_j is the displacement of node j, the

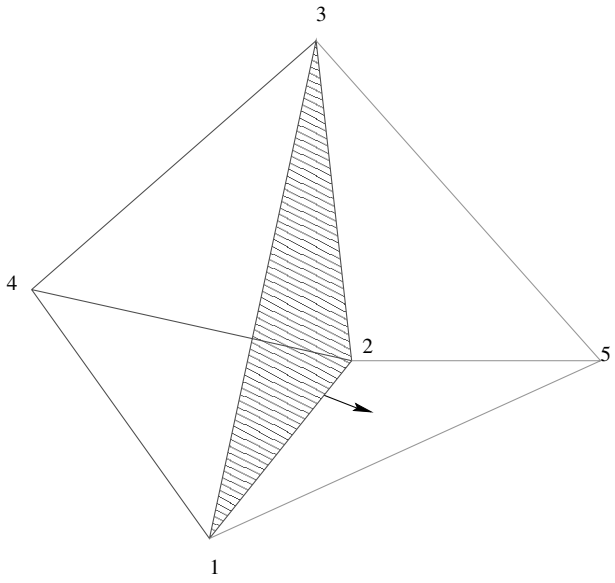

Fig. 2 Evaluation of fluxes in three dimensions.

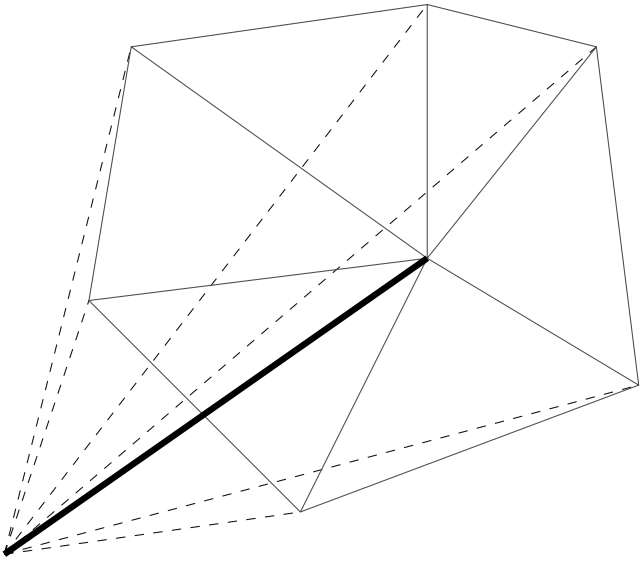

Fig. 3 Control volume for cell-vertex schemes in three dimensions.

opposite end of the edge. The position of static equilibrium of the mesh is computed using a Jacobian iteration with known initial values for the surface displacements.

VII. Overview of Design Process

A flow chart describing the overall design process is shown in Fig. 1.

VIII. Numerical Discretization and Convergence Acceleration Techniques for the Flow and Adjoint Equations

The numerical algorithms and convergence acceleration techniques used in this study to obtain steady-state solutions for the Euler equations are based on a finite element approximation, initially reported in Jameson et al. [20]. The method is described here for completeness. Because of the remarkable similarity between the adjoint system and the flow equations, essentially the same numerical schemes can be reused to obtain the solution to the adjoint system.

The finite element approximation can be obtained by directly approximating the integral equations for the balance of mass, momentum, and energy in polyhedral control volumes. Each of these is formed by the union of the tetrahedra meeting at a common vertex (Fig. 2). It turns out that the flux balance can be broken down into contributions of fluxes through faces in a very elegant way (Fig. 1). This decomposition reduces the evaluation of the Euler equations to a single main loop over the faces. It is shown in Jameson et al. [20] that the same discretization can also be devised from the weak form of the equations using linear trial solutions and test functions. Thus, it is essentially equivalent to a Galerkin method.

Shock waves are captured with the assistance of added artificial dissipation. These shock capturing schemes are derived from a general class of schemes that maintain the positivity of the coefficients, thereby preventing maximas from increasing and minimas from decreasing. The steady-state solutions are obtained by integrating the time-dependent equations with a multistage time stepping scheme. Convergence is accelerated by the use of locally varying time steps, residual averaging, and enthalpy damping.

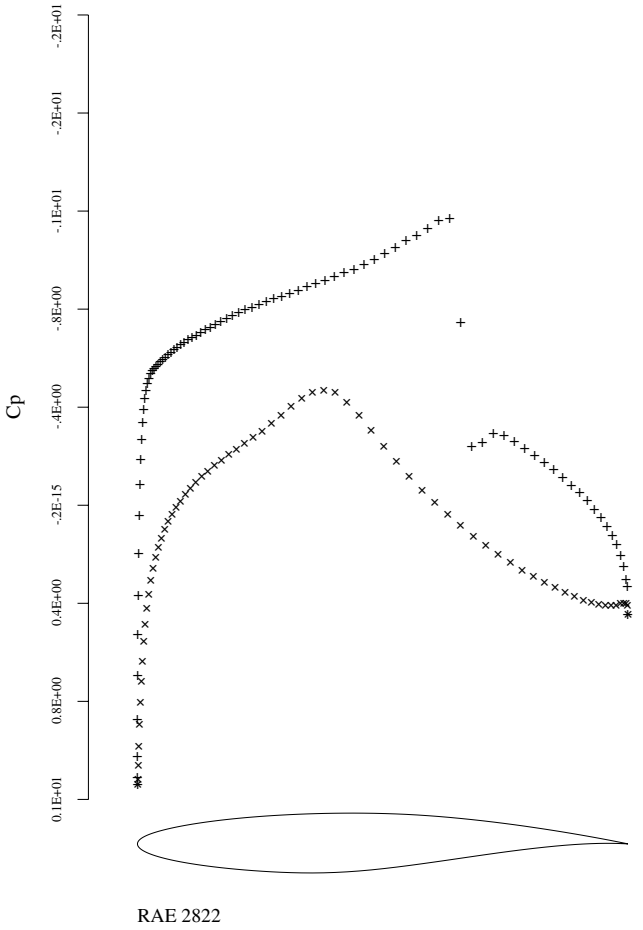

Fig. 4 Initial pressure distribution for the RAE 2822 airfoil.

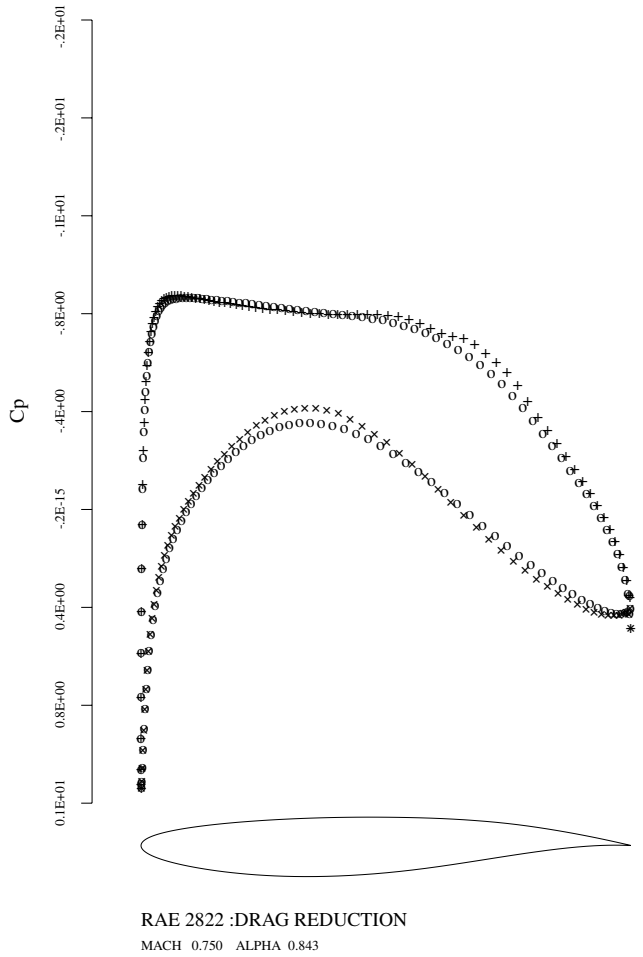

Fig. 5 Pressure distribution as a result of drag minimization for the RAE 2822 airfoil; drag is reduced by 36 counts.

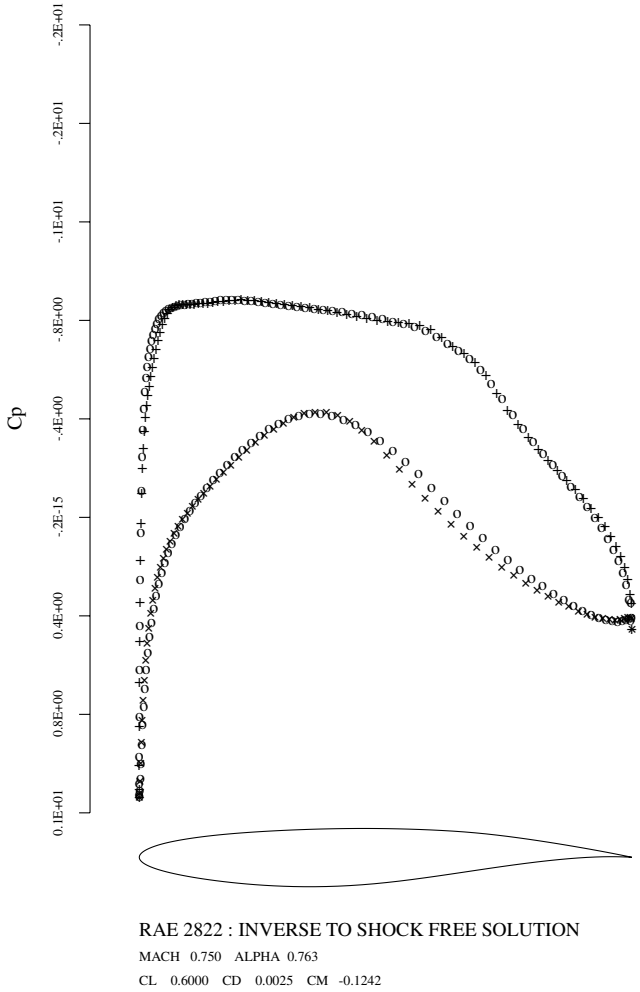

Fig. 6 Attained (+, ×) and target (○) pressure distribution for the RAE 2822 airfoil.

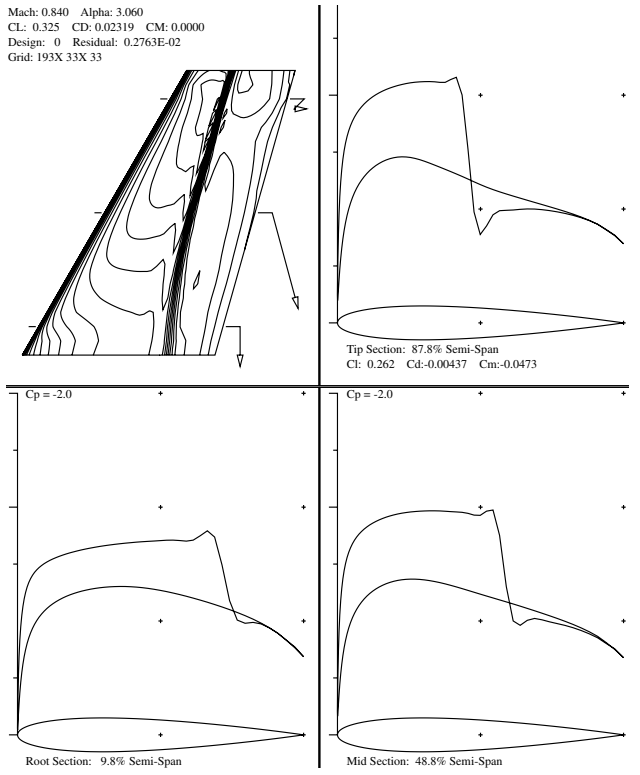

Fig. 7 Initial pressure distribution over a NACA 0012 wing.

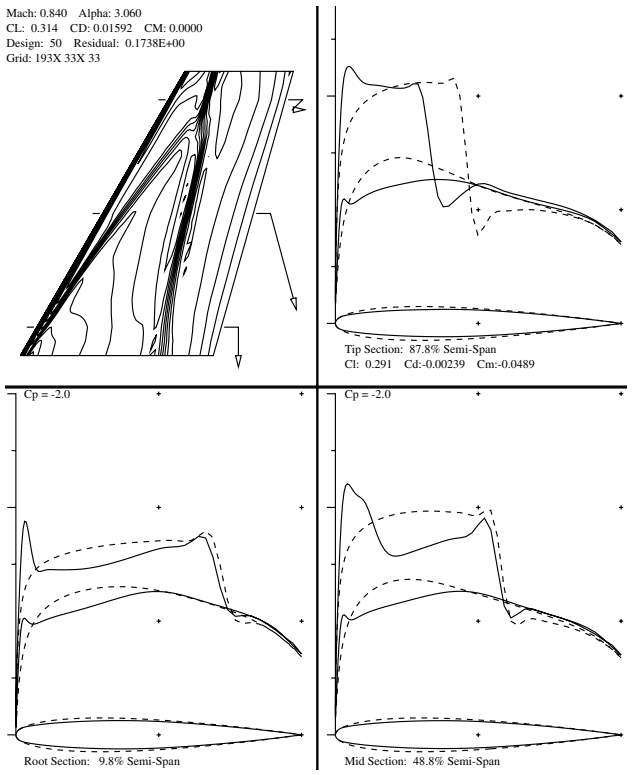

Fig. 8 Initial (dashed lines) and final (solid lines) pressure distribution and modified section geometries.

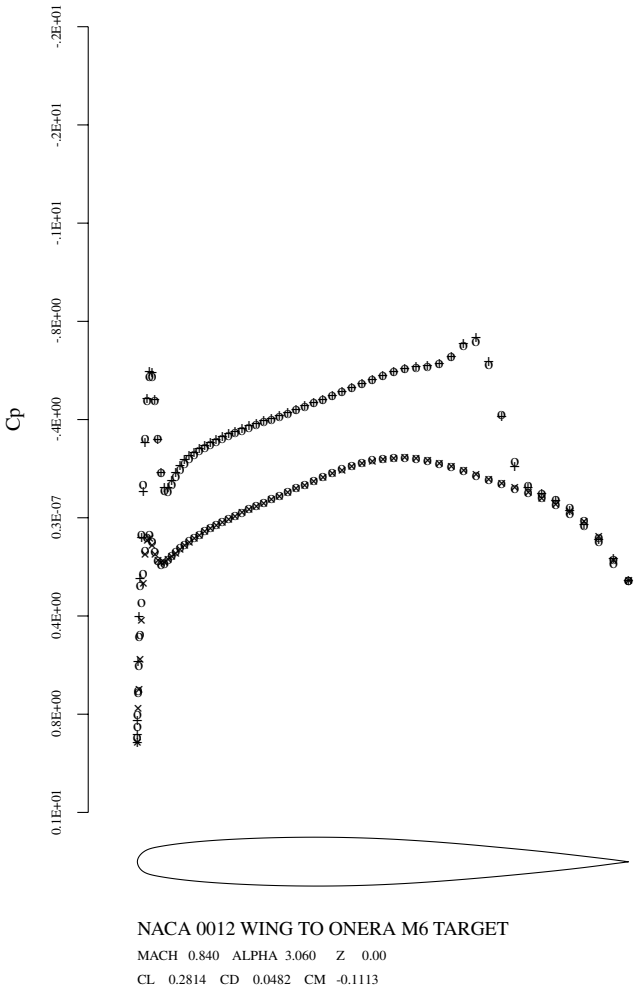

Fig. 9 Attained (+, ×) and target (○) pressure distributions at 0% of the wing span.

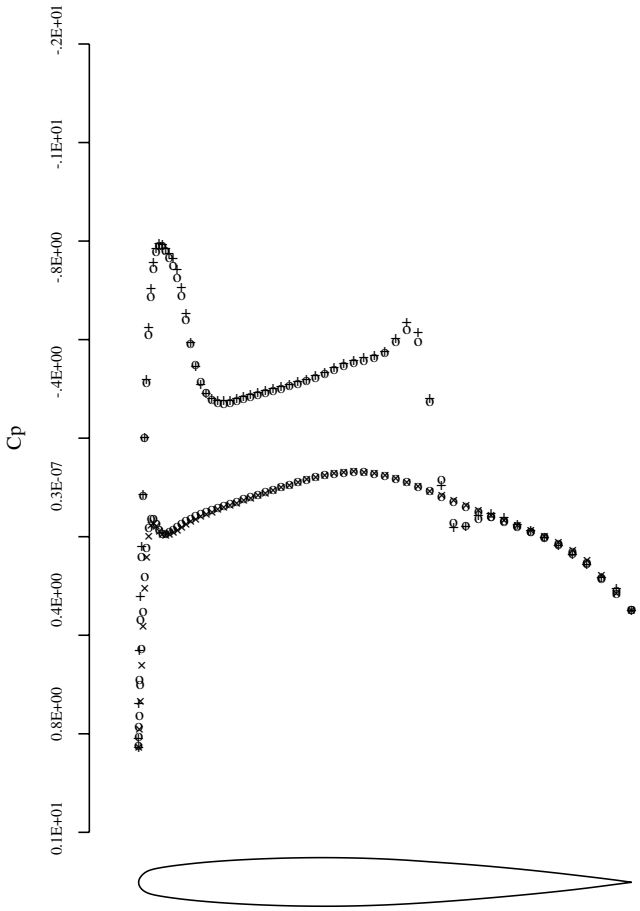

Fig. 10 Attained (+, ×) and target (○) pressure distributions at 40% of the wing span.

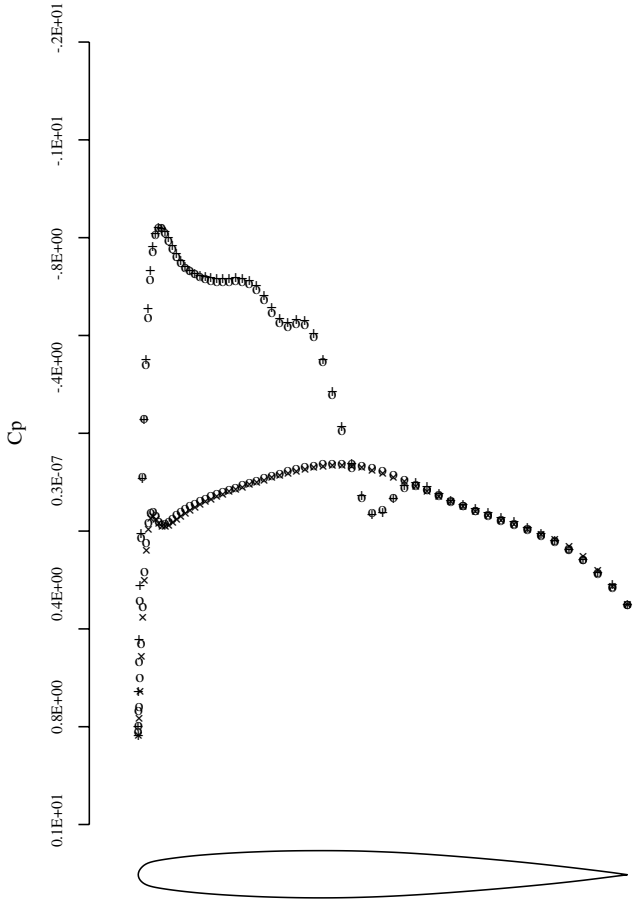

Fig. 11 Attained (+, ×) and target (○) pressure distributions at 80% of the wing span.

Multigrid techniques are also used to further improve convergence to the steady state.

IX. Computational Methodology and Finite Element Approximation

The Euler equations in integral form can be written as

$$\frac{\mathrm{d}}{\mathrm{d}t}\int_V w dV + \int_S F\cdot \mathrm{d}S = 0 \tag{28}$$

Equation (28) can be approximated on a tetrahedral mesh by first writing the flux balance for each tetrahedron assuming the fluxes (F) to vary linearly over each face. Then, at any given mesh point one considers the rate of change of w for a control volume consisting of the union of the tetrahedra meeting at a common vertex. This gives

$$\frac{\mathrm{d}}{\mathrm{d}t}\left(\sum_k V_k w\right) + \sum_k R_k = 0 \tag{29}$$

where V_k is the volume of the kth tetrahedron meeting at a given mesh point and R_k is the flux of that tetrahedron.

When the flux balances of the neighboring tetrahedra are summed, all contributions across interior faces cancel. Referring to Fig. 3, which illustrates a portion of a three-dimensional mesh, it may be seen that with a tetrahedral mesh each face is a common external boundary of exactly two control volumes. Therefore, each internal face can be associated with a set of 5 mesh points consisting of its corners 1, 2, and 3 and the vertices 4 and 5 of the two control volumes on either side of the common face. It is now possible to generate the approximation in Eq. (29) by presetting the flux balance at each mesh point to zero and then performing a single loop over the faces. For each face, one first calculates the fluxes of mass, momentum, and energy across each face, and then one assigns these contributions of the vertices 4 and 5 with positive and negative signs, respectively. Because every contribution is transferred from one control volume into another, all quantities are perfectly conserved. Mesh points on the inner and outer boundaries lie on the surface of their own control volumes, and the accumulation of the flux balance in these volumes has to be correspondingly modified. At a solid surface, it is also necessary to enforce the boundary condition that there is no convective flux through the faces contained in the surface.

Although the original formulation of this method used a face-based loop to accumulate the fluxes, the first author later modified the loops to go through the edges in the mesh as they were typically smaller in number than the faces. The earlier arguments for flux accumulation extend easily to edge-based schemes, and it is this approach that has been used in the current study.

X. Dissipation

A simple way to introduce dissipation is to add a term generated from the difference between the value at a given node and its nearest neighbors. That is, at node 0, we add a term

$$D_o = \sum_k \epsilon_{ko}^{(1)}(w_k - w_o) \tag{30}$$

where the sum is over the nearest neighbors. This contribution is balanced by a corresponding contribution at node k, with the result

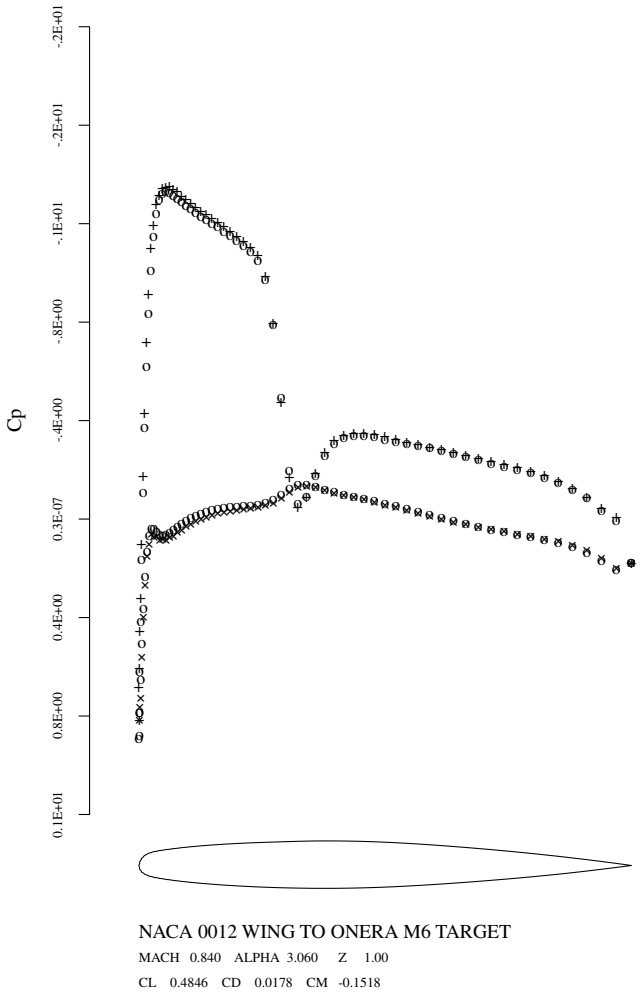

Fig. 12 Final computed and target pressure distributions at 100% of the wing span.

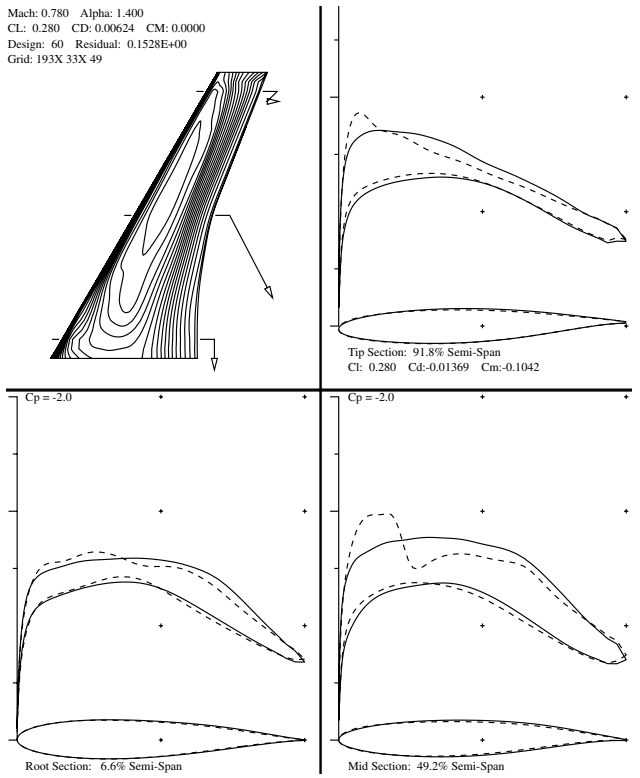

Fig. 13 Initial (dashed lines) and final (solid lines) pressure and section geometries.

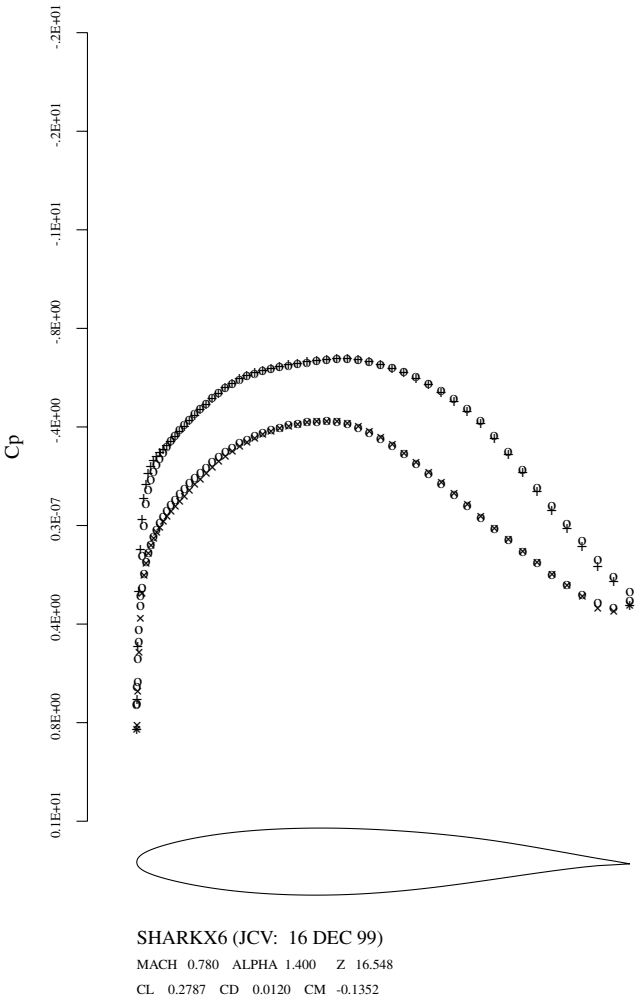

Fig. 14 Attained (+, ×) and target (○) pressure distributions at 5% of the wing span.

that the scheme remains conservative. The coefficients $\epsilon_{ko}^{(1)}$ may incorporate metric information depending on local cell volumes and face areas and can also be adapted to gradients of the solution. As Eq. (30) is only first-order accurate (unless the coefficients are proportional to the mesh spacing), a more accurate scheme is obtained by recycling the edge differencing procedure. After setting

$$E_o = \sum_k (w_k - w_o) \tag{31}$$

at every mesh point, one then sets

$$D_o = -\sum_k \epsilon_{ok}^{(2)} (E_k - E_o) \tag{32}$$

An effective scheme is produced by blending Eqs. (30) and (32) and adapting $\epsilon_{ko}^{(1)}$ to the local pressure gradient. This scheme has been found to have good shock capturing properties, and the required sums can be efficiently assembled by loops over the edges.

Other shock capturing schemes that satisfy the local extremum diminishing property have also been implemented and have been found to work equally efficiently. However, due to the robust nature of the aforementioned simple scalar dissipation model, we have used it for all of the computations in this study.

XI. Integration to Steady State and Convergence Acceleration Techniques

The resulting spatial discretizations yield a set of coupled ordinary differential equations that can be integrated in time to obtain

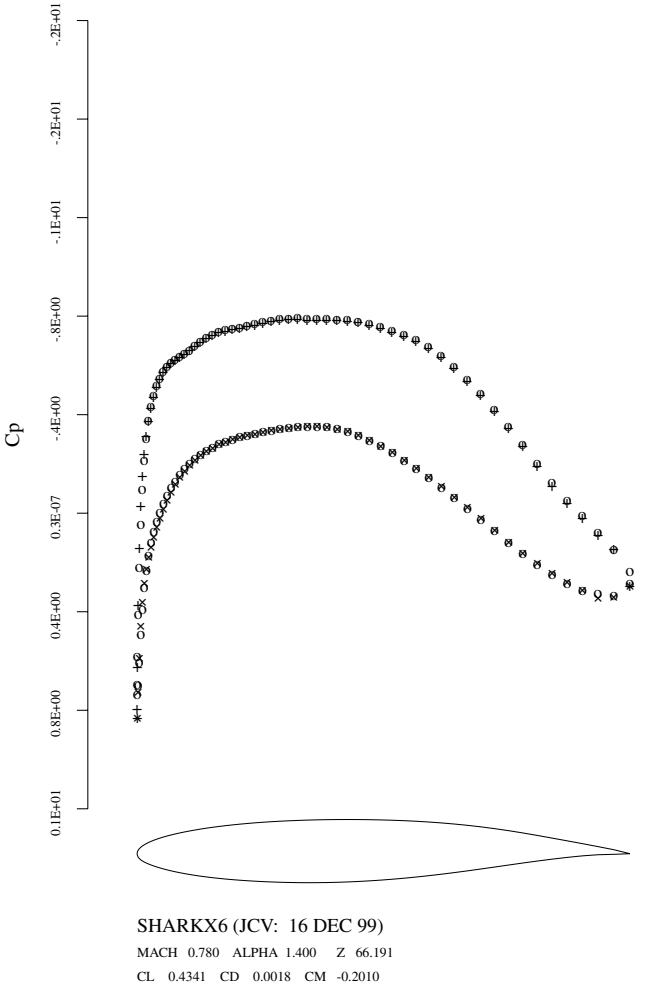

Fig. 15 Attained (+, ×) and target (○) pressure distributions at 50% of the wing span.

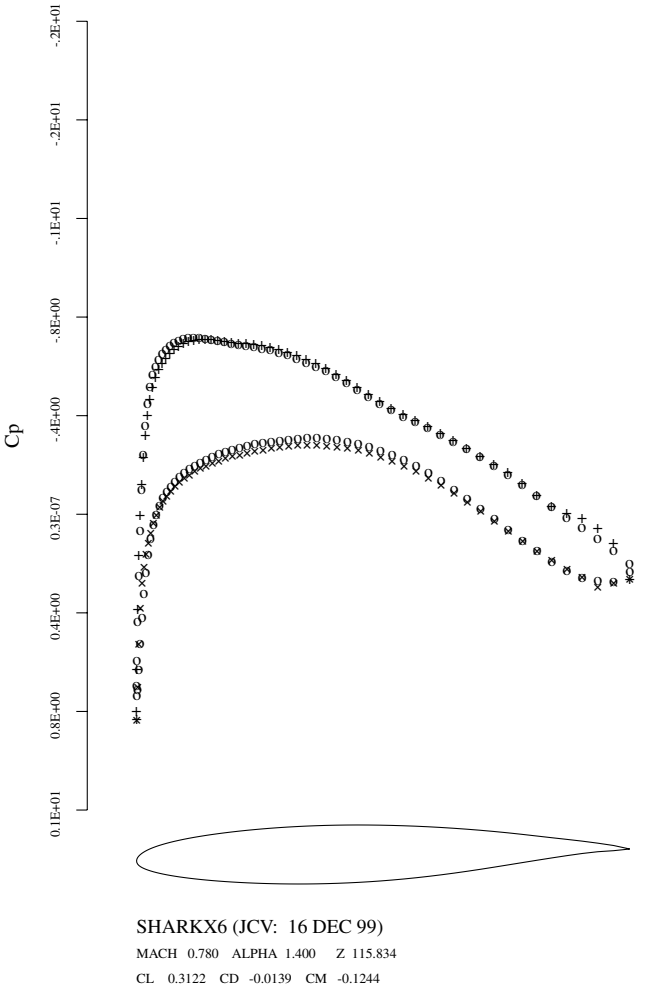

Fig. 16 Initial and final pressure distributions at 95% of the wing span.

steady-state solutions of the Euler equations. To maximize the allowable time step, the same multistage schemes that have proven to be efficient in rectilinear meshes [21] have been used on unstructured meshes. These schemes bear close resemblance to Runge–Kutta schemes with modifications to the evaluation of the dissipation terms that enlarge the stability limit of the scheme along the imaginary axis, thereby allowing convective waves to be resolved.

Convergence to steady state is accelerated by using a variable time step close to the stability limit of each mesh point. The scheme is accelerated further by the introduction of residual averaging [22] and a multigrid procedure [23]. In this study, the coarser grids are either obtained through an independent mesh generator or through an edge-collapsing algorithm. In either approach, transfer coefficients between the various meshes are accumulated in a preprocessing step and recomputed when the meshes are deformed.

XII. Modifications to Numerical Method to Treat Adjoint Equations

To adapt the numerical scheme to treat the adjoint equations, three main modifications are required.

First, because the adjoint equation appears in a nonconservative quasi-linear form, the convective terms have to be calculated in a different manner. The derivatives $\frac{\partial \psi}{\partial x_i}$ are calculated by applying the Gauss theorem to the polyhedral control volume consisting of the tetrahedrons that surround each node. Thus, the formula

$$\frac{\partial \psi}{\partial x_i} = \frac{1}{V} \int_S \psi \, \mathrm{d}S_{x_i} \tag{33}$$

is replaced by its discrete analog, and the contributions are accumulated by edge and face loops in the same manner as the flux balance of Eq. (28). The transposed Jacobian matrices are simplified by using a transformation to the symmetrizing variables. Thus, the

Fig. 17 Density contours for a business jet at $M = 0.8$, $\alpha = 2$.

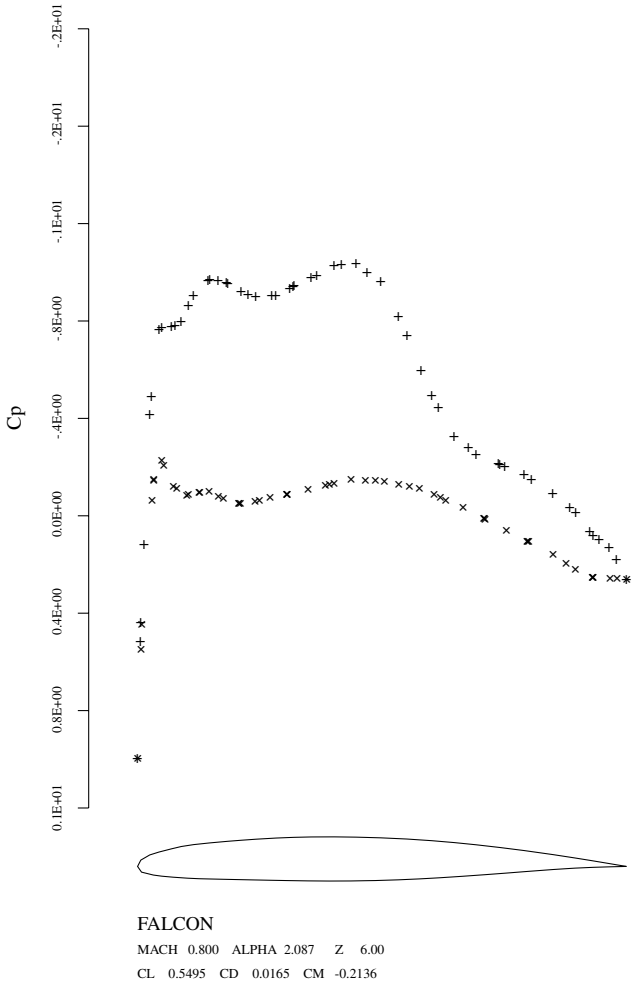

Fig. 18 Pressure distribution at 66% wing span.

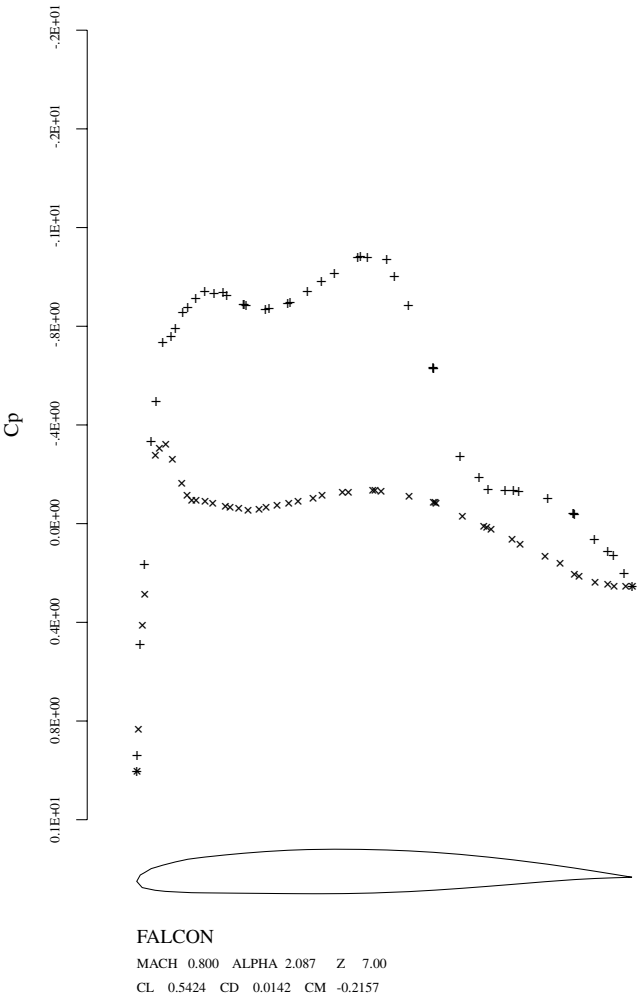

Fig. 19 Pressure distribution at 77% wing span.

Jacobian for flux in the x direction is expressed as

$$A = M\hat{A}M^{-1}, \qquad A^T = M^{-1}\hat{A}M^T$$

where

$$M = \begin{pmatrix} \frac{\rho}{c} & 0 & 0 & 0 & -\frac{1}{c^2} \\ \frac{\rho u}{c} & \rho & 0 & 0 & -\frac{u}{c^2} \\ \frac{\rho v}{c} & 0 & \rho & 0 & -\frac{v}{c^2} \\ \frac{\rho w}{c} & 0 & 0 & \rho & -\frac{w}{c^2} \\ \frac{\rho H}{c} & \rho u & \rho v & \rho w & -\frac{q^2}{2c^2} \end{pmatrix} \tag{34}$$

and

$$\hat{A} = \begin{pmatrix} Q & S_x c & S_y c & S_y c & 0 \\ S_x c & Q & 0 & 0 & 0 \\ S_y c & 0 & Q & 0 & 0 \\ S_z c & 0 & 0 & Q & 0 \\ 0 & 0 & 0 & 0 & Q \end{pmatrix} \tag{35}$$

Second, the direction of time integration to a steady state is reversed because the directions of wave propagation are reversed. Third, although the artificial diffusion terms are calculated by the same subroutines that are used for the flow solution, they are subtracted instead of added to the convective terms to give a downwind instead of an upwind bias. Because of the reversed sign of the time derivatives, the diffusive terms in the time-dependent equation correspond to the diffusion equation with the proper sign.

XIII. Results

The adjoint method described in the previous sections has been applied to two- and three-dimensional problems with the flow modeled by the Euler equations. Both drag reduction and inverse design problems were used to validate the design procedure and the gradient formulations. The method was then used to redesign the shape of the wing of a transonic business jet, where the complete aircraft configuration was modeled. A flow chart describing the overall design process is shown in Fig. 1.

A. Airfoil Design

The unstructured adjoint technology was initially validated for two-dimensional inverse design and drag minimization problems. Figures 4 and 5 show the result of drag minimization for the RAE 2822 airfoil in transonic flow ($M_\infty = 0.75$). The lift was constrained to be 0.6 and the angle of attack was perturbed to maintain the lift. The final geometry is shock free and the drag was reduced by 36 drag counts. Figures 4 and 6 show the result of an inverse design for the RAE 2822 airfoil. Here the target pressure distribution was a shock-free profile obtained from the drag minimization exercise. As can be seen from these pictures, the final pressure profile almost exactly matches the target pressure distribution.

B. Wing Design

The design methodology was then applied to wing shapes in transonic flow. Inverse design computations were performed to validate the design process and the gradient calculations. Figures 7 and 8 show the result of an inverse design calculation, in which the

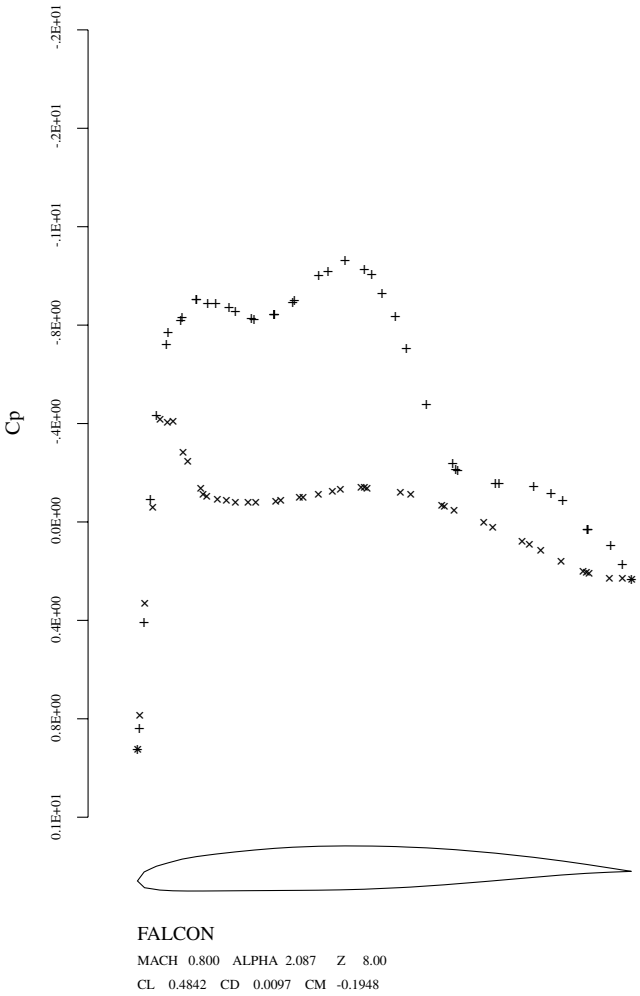

Fig. 20 Pressure distribution at 88% wing span.

initial geometry was a wing with NACA 0012 sections and the target pressure distribution was the pressure distribution over the Onera M6 wing. Figures 9–12 show the target and computed pressure distribution at four spanwise sections. It can be seen from these plots that the target pressure distribution is almost perfectly recovered in 50 design cycles. The results from this test case show that the design process is capable of recovering pressure distributions that are significantly different from the initial distribution and also capturing shocks and other discontinuities in the target pressure distribution.

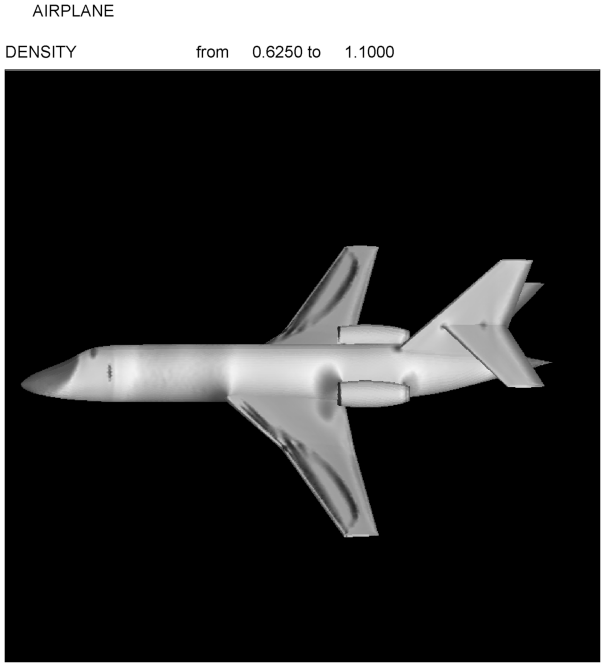

Fig. 21 Density contours for a business jet at $M = 0.8$, $\alpha = 2.3$, after redesign.

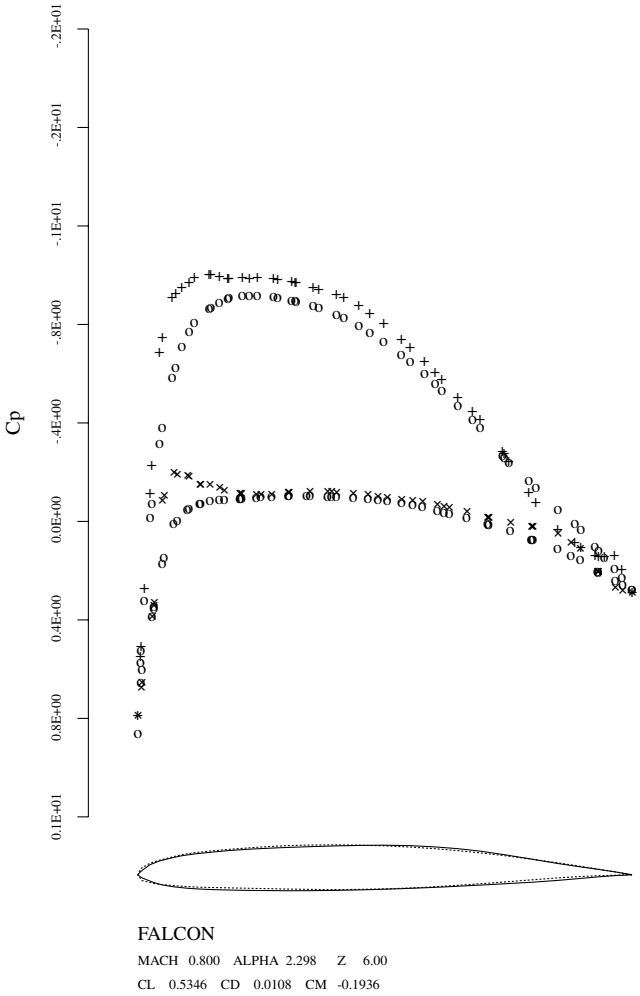

Fig. 22 Pressure distribution at 66% wing span, after redesign (dashed line: original geometry, solid line: redesigned geometry).

Another test case for the inverse design problem used the wing from an airplane (SHARK [24]) that was designed for the Reno Air Races. The initial and target pressure distributions are shown the Fig. 13. As can be seen from these plots, the initial pressure distribution has a weak shock in the outboard sections of the wing. The target pressure distribution is shock free. The computed (after 50 design cycles) and target pressure distributions along three sections of the wing are shown in Figs. 14–16. Again, the design process captures the target pressure with good accuracy in about 50 design cycles.

C. Shape Optimization of Transonic Business Jet

The design method has finally been applied to complete aircraft configurations. As a representative example, we show the redesigns of a transonic business jet to improve its lift to drag ratio during cruise. As shown in Figs. 17–20, the outboard sections of the wing have a strong shock while flying at cruise conditions ($M_\infty = 0.80$, $\alpha = 2$ deg). The results of a drag minimization that aims to remove the shocks on the wing are shown in Figs. 21–24. The drag has been reduced from 235 counts to 215 counts in about eight design cycles. The lift was constrained at 0.4 by perturbing the angle of attack. Further, the original thickness of the wing was maintained during the design

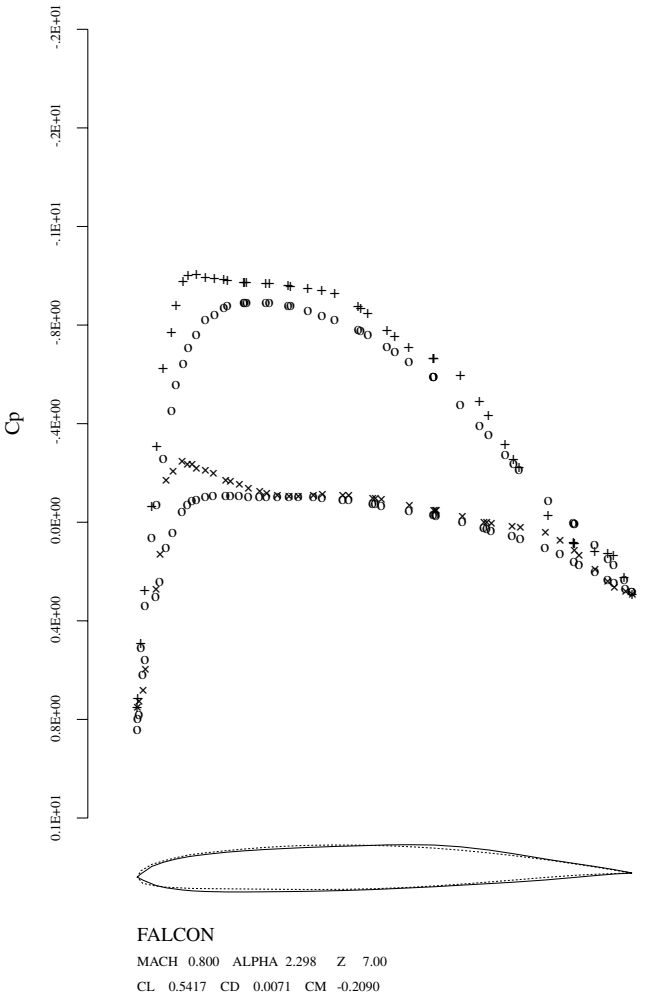

Fig. 23 Pressure distribution at 77% wing span, after redesign (dashed line: original geometry, solid line: redesigned geometry).

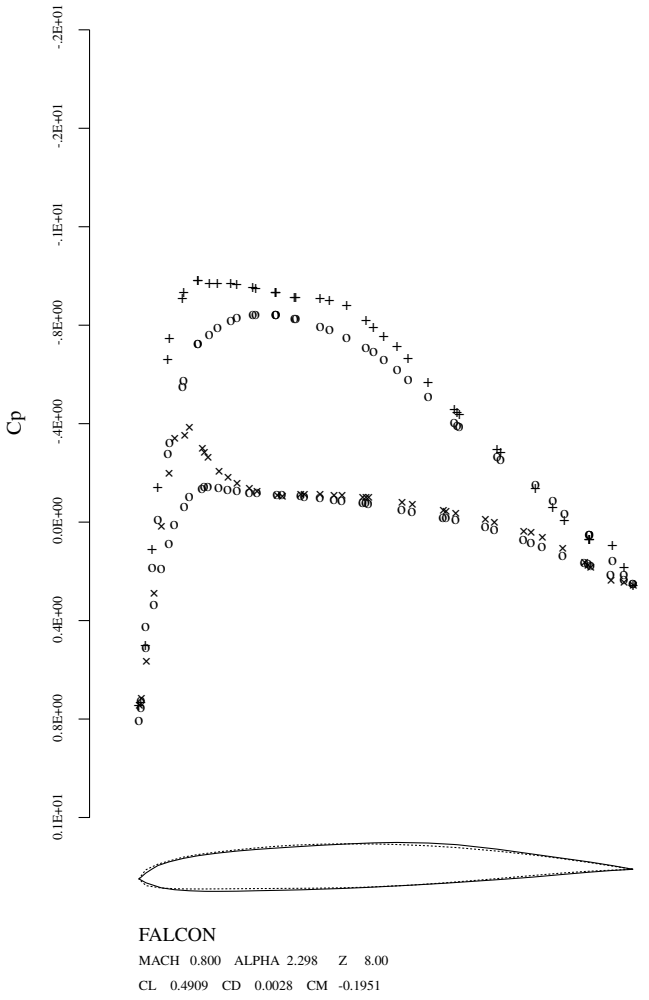

Fig. 24 Pressure distribution at 88% wing span, after redesign (dashed line: original geometry, solid line: redesigned geometry).

process to ensure that fuel volume and structural integrity would be maintained by the redesigned shape. The entire design process typically takes about 4 h on a 1.7 Ghz Athlon processor with 1 Gb of memory. Parallel implementation of the design procedure has also been developed that further reduces the computational cost of this design process.

XIV. Conclusions

The use of gradient formulations that depend only on the surface mesh allows adjoint-based methods to be used for unstructured grids in a computationally efficient manner. Hence, it is now possible to devise a completely automated shape optimization procedure for complete aircraft configurations. Exploiting the flexibility of unstructured grids, it is now possible to tackle wing section and planform optimization, engine integration, and empennage design with an integrated computational procedure. Hence, we believe that this approach holds great promise for airplane design. Extending this approach to viscous flows will enable us to tackle challenging problems in multi-element airfoil optimization using gaps, overlap, and deflections in addition to the shape variables to optimize the geometry. There are two areas of difficulty in using the approach presented in this study. The first pertains to the validation of the reduced gradient formulation for the design variables of interest. The second relates to the robustness of the mesh deformation process during redesign. Both of these problems are currently being investigated by the authors in various contexts, and we hope to present the results of our study in the future.

References

[1] Jameson, A., "Optimum Aerodynamic Design Using Control Theory," *Computational Fluid Dynamics Review*, edited by M. M. Hafez and K. Oshima, Wiley, New York, 1995, pp. 495–528.

[2] Jameson, A., Martinelli, L., and Pierce, N., "Optimum Aerodynamic Design Using the Navier–Stokes Equation," *Theoretical and Computational Fluid Dynamics*, Vol. 10, Nos. 1–4, Jan. 1998, pp. 213–237. doi:10.1007/s001620050060

[3] Jameson, A., "Optimum Aerodynamic Design via Boundary Control," Research Institute of Advanced Computer Science Technical Report 94.17, May 1994; also Princeton University Report MAE 1996; also *Proceedings of AGARD FDP/Von Karman Institute Special Course on "Optimum Design Methods in Aerodynamics"* Brussels, April 1994, pp. 3.1–3.33.

[4] Jameson, A., and Martinelli, L., *Aerodynamic Shape Optimization Techniques Based on Control Theory*, Lecture Notes in Mathematics, Springer, Berlin, 2000.

[5] Jameson, A., Alonso, J. J., Reuther, J., Martinelli, L., and Vassberg, J. C., "Aerodynamic Shape Optimization Techniques Based on Control Theory," AIAA Paper 98-2538, June 1998.

[6] Nadarajah, S. K., and Jameson, A., "Optimal Control of Unsteady Flows Using a Time Accurate Method," AIAA Paper 2002-5436, Sept. 2002.

[7] Leoviriyakit, K., and Jameson, A., "Aerodynamic Shape Optimization of Wings Including Planform Variations," AIAA Paper 2003-0210, Jan. 2003.

[8] Reuther, J. J., Alonso, J. J., Jameson, A., Rimlinger, M. J., and Saunders, D., "Constrained Multipoint Aerodynamic Shape Optimization Using an Adjoint Formulation and Parallel Computers: Parts 1, 2," AIAA Paper 97-0103; also *Journal of Aircraft*, Vol. 36, No. 1, Jan.–Feb. 1999, pp. 51–60, 61–74.

[9] Cliff, S., Reuther, J., Sanders, D., and Hicks, D., "Single and Multipoint Aerodynamic Shape Optimization of High Speed Civil Transport," *Journal of Aircraft*, Vol. 38, No. 6, Nov.–Dec. 2001, pp. 997–1005.

[10] Pironneau, O., *Optimal Shape Design for Elliptic Systems*, Springer–Verlag, New York, 1984.
[11] Lions, J. L., *Optimal Control of Systems Governed by Partial Differential Equations*, translated by S. K. Mitter, Springer–Verlag, New York, 1971.
[12] Jameson, A., Schmidt, W., and Turkel, E., "Numerical Solution of the Euler Equations by Finite Volume Methods Using Runge–Kutta Time Stepping Schemes," AIAA Paper 81-1259, June 1981.
[13] Jameson, A., and Baker, T. J., "Improvements to the Aircraft Euler Method," AIAA Paper 87-0353, Jan. 1987.
[14] Barth, T. J., "Aspects of Unstructured Grids and Finite Volume Solvers for the Euler and Navier–Stokes Equations," AGARD, *Special Course on Unstructured Grid Methods for Advection Dominated Flows*, edited by T. E. Tezduyar, May 1992.
[15] Elliot, J., and Peraire, J., "Aerodynamic Design Using Unstructured Meshes," AIAA Paper 96-1941, Jan. 1996.
[16] Anderson, K., and Venkatakrishnan, V., "Aerodynamic Design Optimization on Unstructured Grids Using a Continuous Adjoint Formulation," AIAA Paper 97-0643, Jan, 1997.
[17] Cliff, S. E., Thomas, S. D., Baker, T. J., Jameson, A., and Hicks, R. M., "Aerodynamic Shape Optimization Using Unstructured Grid Method," AIAA Paper 02-5550, Sept. 2002.
[18] Jameson, A., and Kim, S., "Reduction of the Adjoint Gradient Formula in the Continuous Limit," AIAA Paper 2003-0040, Jan. 2003.
[19] Jameson, A., Martinelli, L., and Vassberg, J. C., "Using Computational Fluid Dynamics for Aerodynamics—A Critical Assessment," *23rd International Congress of Aeronautical Sciences*, 8–13 Sept. 2002, Toronto, Canada.
[20] Jameson, A., Baker, T. J., and Weatherill, N. P., "Calculation of Inviscid Transonic Flow over a Complete Aircraft," AIAA Paper 86-0103, Jan. 1986.
[21] Jameson, A., "Transonic Flow Calculations," Princeton Univ., Mechanical and Aerospace Engineering Rept. 1651, 1991.
[22] Pulliam, T. H., and Steger, J. L., "Implicit Finite Difference Simulations of Three Dimensional Compressible Flow," *AIAA Journal*, Vol. 18, No. 2, 1980, pp. 159–167.
[23] Jameson, A., Mavriplis, D. J., and Martinelli, L., "Multigrid Solution of the Navier–Stokes Equations on Triangular Meshes," Institute for Computer Applications in Science and Engineering Rept. 89-11, 1989; also AIAA Paper 89-0283, Jan. 1989.
[24] Ahlstrom, E., Gregg, R., Vassberg, J., and Jameson, A., "G-Force: The Design of an Unlimited Class Reno Racer," AIAA Paper 2000-4341, Aug. 2000.

K. Fujii
Associate Editor